Human Molecular Genetics, 2005, Vol. 14, No. 23 ***3565–3577***
doi:10.1093/hmg/ddi384
Advance Access published on October 13, 2005

Inactivation of the peroxisomal ABCD2 transporter in the mouse leads to late-onset ataxia involving mitochondria, Golgi and endoplasmic reticulum damage

Isidre Ferrer[1], Josef P. Kapfhammer[2], Colette Hindelang[3], Stephan Kemp[4], Nathalie Troffer-Charlier[3], Vania Broccoli[5], Noëlle Callyzot[6,†], Petra Mooyer[4], Jacqueline Selhorst[3,4], Peter Vreken[4], Ronald J.A. Wanders[4], Jean Louis Mandel[3] and Aurora Pujol[7,*]

[1]Institut de Neuropatologia, Hospital Universitari de Bellvitge, Departament de Biologia Cel.lular i Anatomia Patologica, Facultat de Medicina, Universitat de Barcelona, IDIBELL c/Feixa Llarga s/n E-08907 L'Hospitalet de Llobregat, Barcelona, Spain, [2]Anatomisches Institut, Universität Basel, Pestalozzistr. 20, CH-4056 Basel, Switzerland, [3]Institut de Génétique et de Biologie Moléculaire et Cellulaire, CNRS/INSERM/ULP and Collège de France, B.P. 10142, 67404 Illkirch Cedex, C.U. de Strasbourg, France, [4]Laboratory of Genetic Metabolic Diseases, Department of Clinical Chemistry and Department of Pediatrics, Emma Children's Hospital, Academic Medical Center, University of Amsterdam, PO Box 22700, 1100 DE Amsterdam, The Netherlands, [5]Stem Cell Research Institute, DIBIT, San Raffaele Science Park, Via Olgettina 58, Milan, Italy, [6]Societé Neurofit, SA 67404 Illkirch Cedex, C.U. de Strasbourg, France and [7]Istitució Catalana de Recerca i Estudis Aplicats (ICREA) and Centre de Genètica Mèdica i Molecular, IRO/IDIBELL, Gran Via s/n, km 2.7, 08907 L'Hospitalet de Llobregat, Barcelona, Spain

Received July 12, 2005; Revised and Accepted October 6, 2005

ATP-binding cassette (ABC) transporters facilitate unidirectional translocation of chemically diverse substances, ranging from peptides to lipids, across cell or organelle membranes. In peroxisomes, a subfamily of four ABC transporters (ABCD1 to ABCD4) has been related to fatty acid transport, because patients with mutations in ABCD1 (*ALD* gene) suffer from X-linked adrenoleukodystrophy (X-ALD), a disease characterized by an accumulation of very-long-chain fatty acids (VLCFAs). Inactivation in the mouse of the *abcd1* gene leads to a late-onset neurodegenerative condition, comparable to the late-onset form of X-ALD [Pujol, A., Hindelang, C., Callizot, N., Bartsch, U., Schachner, M. and Mandel, J.L. (2002) Late onset neurological phenotype of the X-ALD gene inactivation in mice: a mouse model for adrenomyeloneuropathy. *Hum. Mol. Genet.*, 11, 499–505.]. In the present work, we have generated and characterized a mouse deficient for *abcd2*, the closest paralog to *abcd1*. The main pathological feature in abcd2−/− mice is a late-onset cerebellar and sensory ataxia, with loss of cerebellar Purkinje cells and dorsal root ganglia cell degeneration, correlating with accumulation of VLCFAs in the latter cellular population. Axonal degeneration was present in dorsal and ventral columns in spinal cord. We have identified mitochondrial, Golgi and endoplasmic reticulum damage as the underlying pathological mechanism, thus providing evidence of a disturbed organelle cross-talk, which may be at the origin of the pathological cascade.

*To whom correspondence should be addressed at: CGMM, IRO/IDIBELL, Hospital Duran i Reynals, Gran Via s/n, km 2.7, 08907 L'Hospitalet de Llobregat, Barcelona, Spain. Tel: +34 932607425; Fax: +34 932607414; Email: apujol@iro.es
†Present address: Phytopharm PLC, Cambridge, England.

INTRODUCTION

Peroxisomes are subcellular organelles present in most eukaryotic cells (1). They fulfill a number of essential cellular functions, including the catabolism of pipecolic, phytanic and very-long-chain fatty acids (VLCFAs) and the biosynthesis of plasmalogens (ether lipids) and bile acids (2). The importance of peroxisomes for normal cellular functioning is illustrated by the peroxisome biogenesis disorders (PDB) (Zellweger syndrome, neonatal adrenoleukodystrophy and infantile Refsum's disease). PBDs are characterized by a loss of functional peroxisomes, resulting in the presence of matrix enzymes in the cytosol because of mutations in one of the many so-called *PEX* genes, which encode proteins (peroxins) essential for proper peroxisome biogenesis (3,4). In Zellweger syndrome, the most severe of these disorders, infants exhibit neonatal hypotonia, hepatic dysfunction and seizures associated with neuronal migration defects (McKusick 214100). Indeed, in the nervous system, peroxisomes have been localized in cell bodies, axons, dendrites, neurites and presynaptic axon terminals (5–8) and active growth cones (9), suggesting an active metabolic role for peroxisomes in guidance cues, in outgrowth and in maintenance of neurites.

ATP-binding cassette (ABC) transporters constitute a family of transport proteins that couple the energy of ATP hydrolysis to the translocation of a wide variety of substrates, such as ions, proteins, sugars, amino acids and lipids, across biological membranes (10,11). In peroxisomes, four genes coding for ABC transporters have been identified (*ABCD1* to *ABCD4*). Mutations in ABCD1 results in X-linked adrenoleukodystrophy/adrenomyeloneuropathy (X-ALD/AMN) (12). To date, no human disease has been attributed to defects in the genes coding for ALDRP (*ABCD2*), PMP70 (*ABCD3*) or PMP69 (*ABCD4*). Patients with X-ALD are characterized biochemically by elevated levels of VLCFA because of a defect in peroxisomal β-oxidation of VLCFAs. Because of the biochemical phenotype of X-ALD patients, it has been postulated that the product of the *ABCD1* gene, i.e. ALDP, may import VLCFAs into the peroxisome. This is supported by the observation that yeast lacking one or both of the two yeast ABCD transporters (Pxa1p and Pxa2p) have elevated VLCFA levels (13,14). The functions of the three other transporters in higher eukaryotes are unknown, but their sequence homology (88% for ABCD1 and ABCD2; 66% for ABCD1 and ABCD3 or ABCD4) indicate that they might exert related or overlapping function(s) in peroxisomal fatty acid metabolism. For instance, PMP70 and ALDRP have been shown to compensate for the loss of ALDP when overexpressed *in vitro* (15,16). However, the intrinsic function of PMP70 as evaluated in abcd3−/− mice, has recently been reported to be related to the catabolism of middle- and branched-chain fatty acids (pristanic and phytanic), in the absence of VLCFAs accumulation (17). Similarly, inactivation of *abcd2* does not lead to accumulation of VLCFAs in nervous tissues, although its stable overexpression by transgenesis in the ALD knoc-kout mouse prevents accumulation of VLCFAs as well as the onset of neurological phenotype (18), which indicates that ALDRP is indeed able to take over from ALDP, at least when overexpressed. In the present study, we set up to explore in-depth the intrinsic role of ALDR.

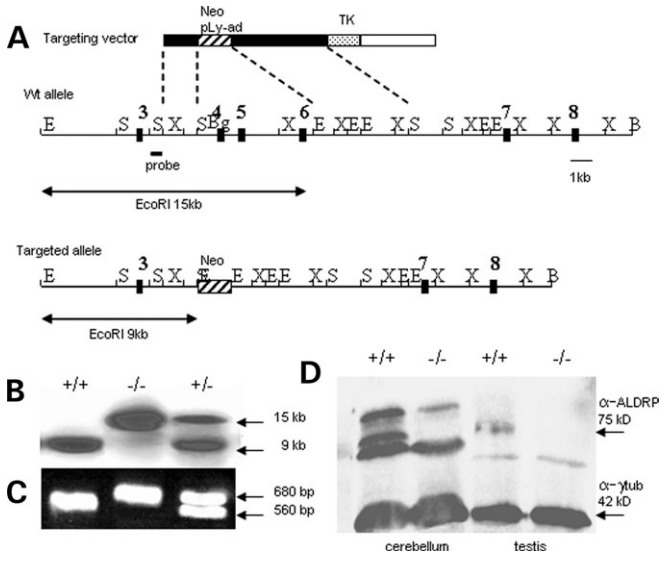

Figure 1. Abcd2 knock-out strategy and construct. (**A**) Wild-type endogenous mouse Abcd2 locus. DNA targeting construct used for gene targeting in ES cells to create a knock-out allele, lacking exons 4–6 and harboring the neomycin cassette (Neo) after site-specific recombination. A modified neomycin cassette was inserted, replacing the coding portions of exons 4–6. (**B**) Southern blot analysis demonstrating homologous recombination at the Abcd2 locus in mouse tail genomic DNA. Southern blots are shown using an external flanking probe on *Eco*RI digested genomic DNA. (**C**) PCR fragments for mouse genotyping. (**D**) Western blot analysis of ABCD2 protein in lysates of cerebellum and testis, prepared from aldr−/− mice and wild-type littermates. γ-Tubulin is used as loading control.

RESULTS

Generation of abcd2 null mutant mice (abcd2−/−)

Mouse strains with a targeted deletion of exons 4–6 of the mouse *abcd2* gene (Fig. 1A) were generated from two independent ES clones (Material and Methods). To verify that the targeted genetic disruption of *abcd2* resulted in a null allele, we performed RT-PCR experiments and ALDRP protein analyses with a C-terminal antibody, as described subsequently (18). Western blots showed a complete absence of the protein in all tissues of abcd2−/− mice (Fig. 1D). Quantitative RT-PCR confirmed the absence of full-length *abcd2* mRNA, although shorter, smir-type and low expressed fragments could be detected, consistent with nonsense-mediated mRNA decay process (data not shown). Absence of the *abcd2* gene was not accompanied by compensatory increases of its closest paralog, the *abcd1* gene, as evidenced by quantitative PCR experiments on whole extract CNS, PNS, adrenal gland and testis samples (data not shown).

The progeny derived from the two ES clones were kept independent and used separately in the study. Because the results were identical, the experimental data obtained with both strains were combined. Mice lacking the *abcd2* gene were delivered in expected Mendelian ratios, were viable and fertile and did not show any obvious abnormalities in development, behavior or gross morphology of the nervous system up to 6 months (data not shown).

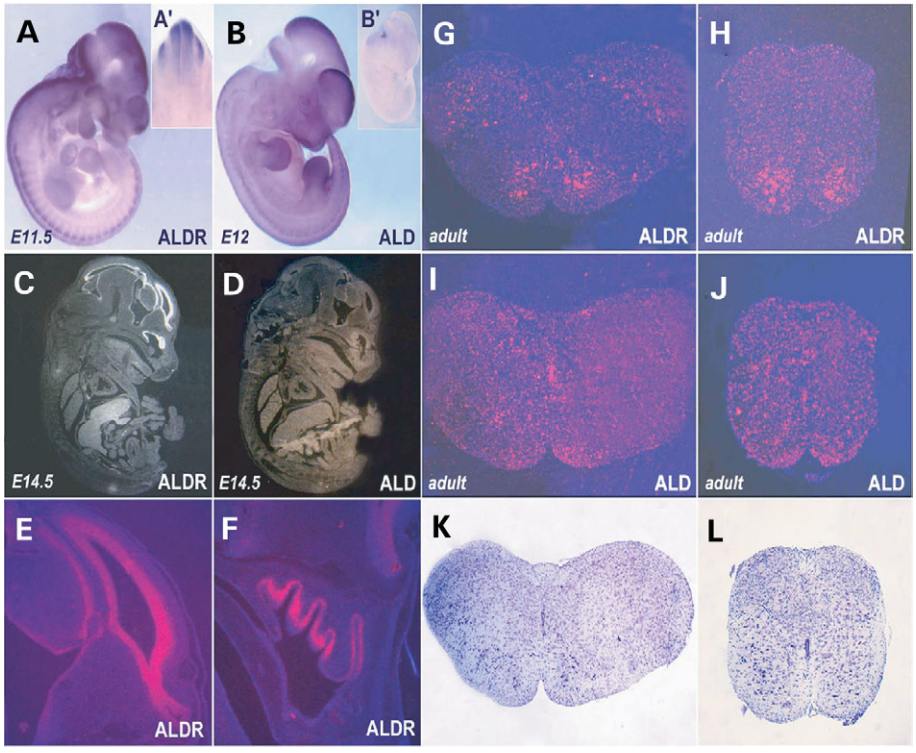

Figure 2. *Ald* and *Aldr* RNA expression in early and mid-embryonic stages (**A**–**F**) and adult pons and spinal cords (**G**–**L**). (A) *Aldr* is strongly expressed in DRGs at E11 and 5. Proliferative neurons in cortex (C and E) and neuro-olfactive epitelium (F) are strongly positive for *aldr* at E14 and 5. In adult stages (weeks 5–6), *aldr* is expressed in interneurons of pons (G) and spinal cord (H). In contrast, the *ald* gene exhibits a low and ubiquitous expression pattern, throughout embryonic development (B and D) and adult pons (I) and spinal cord (J).

Expression pattern of *abcd1* and *abcd2* genes

We have shown in a previous study that the expression of both transporters was mirror-like or complementary in adrenal gland and testis. In the brain, *abcd2* mRNA was detected mainly in pyramidal and granular cell layers of dentate gyrus and cerebral cortex. The inner granular and Purkinje cell layers in cerebellum were also strongly labeled for *abcd2*. In contrast, *abcd1* expression was essentially restricted to glial and endothelial cells (19). Here, we aimed at refining *abcd2* mRNA expression pattern during embryonic life and in early adulthood (Fig. 2). *Abcd2* appears well expressed in dorsal root ganglia (DRG) (sensitive peripheral neurons) in early embryonic stages (E11 and 5) (Fig. 2A) and in proliferative neuronal layers from cerebral cortex and neuro-olfactory epithelium at mid-embryonic stages (Fig. 2C, E and F, at E14 and 5). In adult spinal cord and pons, motor neurons, interneurons and basal ganglia are strongly positive for *abcd2* (Fig. 2G and H). In summary, *abcd2* is widely expressed in different types of neuronal populations, from embryonic sensitive neurons of DRGs to mature differentiated spinal motor neurons. In contrast, *abcd1* exhibited a low and ubiquitous expression pattern throughout development into adulthood, without being excluded from neurons.

Behavioral deficits in ALDRP-deficient mice

To assess the neurological consequences of ALDRP/ABCD2 absence, mutant animals were analyzed using a variety of motor skills and behavioral tests. Although no overt clinical phenotype was observed at 6 months, mice lacking ALDRP displayed progressive behavioral deficits, consistent with ongoing neural degeneration from 12 months onwards. The most striking abnormalities were found in the areas of balance, coordination and reflexes. The rotarod test was used as a measure of motor balance, coordination and control. When compared with wild-type littermates at 12 months of age, abcd2−/− mice displayed a marked impairment in their performance during 4 days trial on the rotating rod set at an accelerating speed ($P < 0.01$ by ANOVA) (Fig. 3B). Abcd1-mice performed similar to their wild-type littermates at this age (data not shown). Latter in life, around 20 months, cohorts of mice from all genotypes were again challenged. The performance of *abcd2* null mice was even more impaired, and a slight whole body tremor suggestive of cerebellar involvement was apparent in three out of 14 abcd2−/− mice and in eight out of 11 abcd1−/abcd2−/− double mutant mice. Data are in agreement with the rotarod experiments reported in a former study (18) (data not shown).

We studied spontaneous locomotion and exploratory behavior in the open field at 12 months of age. Surprisingly, despite their impaired performance in rotarod tests, abcd2−/− null mice were significantly more active than their wild-type littermates. This was especially apparent after the first 5-min period (Fig. 3A). This finding is indicative of a lack of habituation capacity to a new environment. Interestingly, abcd1 knock-out mice and particularly double mutants exhibited a

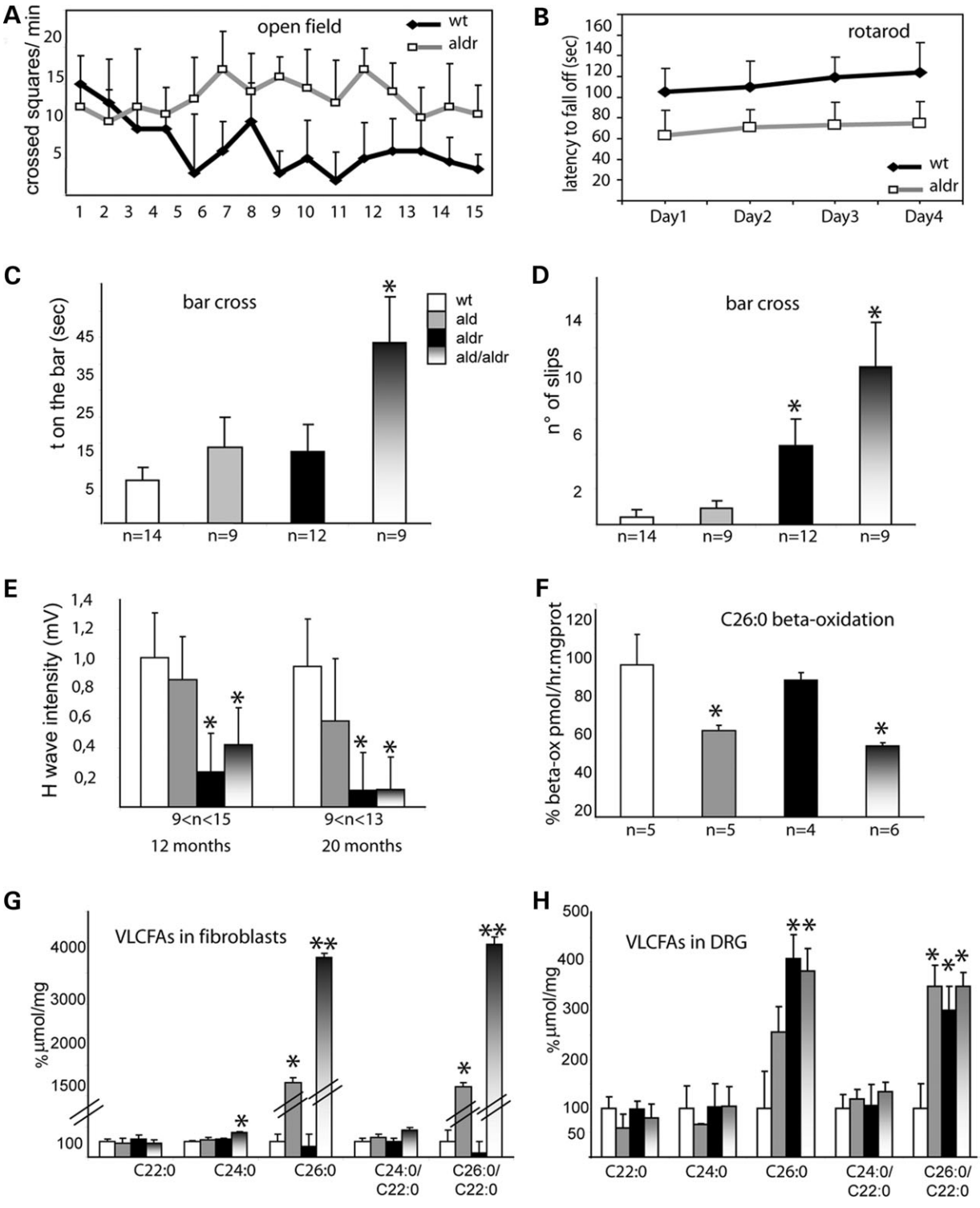

Figure 3. Aldr−/− mice present a progressive neurological phenotype. (**A**) Open-field experiments showing lack of habituation of aldr−/− mutants at 12 months of age ($n = 8$ wt and $n = 12$ aldr−/−). (**B**) Rotarod analysis of mutants versus control littermates, same age (**C** and **D**, bar cross test). (C) The time spent to cross the bar. (D) The number of slips. Aldr−/− slipped away more often than their wild-type littermates and ald-mice. Double mutant animals show delayed time to cross the bar and increased number of slips. (**E**) Electromyographical measurements of the spinal somatosensory evoked response (H-wave or reflex wave) in aldr−/−, ald− and double mutant versus control littermates at 12 and 20 months of age. The absence of H-wave is aldr dependent. (**F**) Capacity of adult fibroblasts to β-oxidize C26:0, expressed as picomoles per hour per milligram of protein. Wild-type levels have been set to 100. Ald− and double mutant fibroblasts show similar reduction to 60% of the wild-type level ($P < 0.0008$). (**G** and **H**) Quantification of saturated VLCFA levels by ESI-MS in adult fibroblasts and DRG samples, expressed as micromoles per milligram of protein. Wild-type levels have been set to 100. (Single asterisk) Significant difference versus wild-type. (Double asterisks) Significant difference versus ald− samples (when ald− is different against wild-type). All statistics by ANOVA (Statview Package 5, significance set at $P < 0.01$).

decline in deambulation activity when compared with wild-types, and significantly poorer rearing behaviors, latter in life (20 months) (18).

At 15 months of age, the time required for mice to reach a platform along a balance bar was significantly increased in abcd1−/abcd2−/− double mutants ($P < 0.001$) (Fig. 3C). Both abcd2−/− and abcd1−/abcd2−/− mice exhibited a marked tendency to slip off the bar, a sign of ataxia (Fig. 3D), and often failed to maintain balance and fell. Instead of walking and maintaining a stable upright posture, they displayed ventral recumbence, with their entire body flattened against the surface of the bar, and their hind and fore limbs wrapped laterally around the bar. They used their fore limbs to drag themselves along the beam, being their hind limbs generally not used. This sign was particularly evident in double mutant mice. At 20 months of age, six out of 11 double mutant mice were not able to perform the test, because they 'froze' or fell repeatedly from the bar (data not shown). These subsets of mice that showed a more severe phenotype exhibited, in addition, exaggerated bilateral extension of fore and hind limbs when suspended by their tails. We detected postural hypotonia, characterized by animals lying flat on their abdomen with fore and hind limbs splayed laterally. Because this effect could be caused by inhibition of postural muscle tone (20), we measured muscular strength with a dynamometer. No difference could be demonstrated between mutants and controls (data not shown), thus excluding any gross influence of muscle weakness on their rotarod or bar cross performance.

Defective spinal reflex in abcd2−/− mice

We assessed function of the peripheral nervous system by electromyographical exploration after somatosensory stimulation of the sciatic nerve. ALDP deficient mice present altered motor and sensitive conduction velocities (21). These deficits were not found in abcd2 mutants. Here, we investigated an additional parameter, the spinal somatosensory response or spinal reflex (H-wave amplitude). At 12 months of age, *abcd2*−/− mice present lower amplitude of the H-wave than their wild-type littermates (Fig. 3E). Latency of the H-wave is normal at that age, but diminishes with age (Fig. 3E). In contrast, this loss of spinal reflex is not presented by abcd1 mutants, which have values comparable to wild-types even at older ages. Double mutants exhibit comparable deficits in amplitude and latency parameters to abcd2−/− mice. These results indicate that the large proprioceptive sensory neurons at DRG or their afferents are functionally defective and are consistent with ataxia and loss of propioception evidenced at the bar cross and rotarod tests.

Biochemical function of ALDRP

Given the high sequence homology and the differential expression pattern of both proteins, we speculated that ALDP and ALDRP could play similar or overlapping biochemical functions in different cell types. Indeed, upon overexpression, ALDRP has been shown to compensate for ALDP loss *in vitro* and *in vivo*. In X-ALD patient fibroblasts, transient overexpression of ALDR cDNA corrects the biochemical defect and transgenic overexpression of ALDRP in abcd1-mice prevents the VLCFAs accumulation in target tissues (18). However, saturated VLCFAs do not accumulate in adult brain, spinal cord and sciatic nerve of abcd2−/− mice (18). Here, we have investigated saturated VLCFA levels and C26:0 β-oxidation capacity on adult fibroblasts derived from our different mouse mutants. In this cell type, lack of ALDRP is neither translated into an accumulation of VLCFAs nor into a decrease of C26:0 β-oxidation capacity (Fig. 3G and H). Interestingly, double mutant fibroblasts accumulate higher levels of C26:0 than abcd1-fibroblasts ($P < 0.001$). In addition, C24:0 levels are higher in double mutants than in wild-type or abcd1-fibroblasts ($P < 0.01$). This suggests that *abcd2* might cooperate or compensate to some extent for *abcd1* loss of function. This functional compensation does not occur through of an increase of abcd2 expression at the mRNA or protein levels (data not shown).

Seeking for an alternative consequence of ALDRP loss of function different from VLCFAs accumulation, we set out to determine levels of other peroxisomal metabolites. We quantified phytanic and pristanic acids in plasma and liver and the plasmalogens C16:0 DMA and C18:0 DMA in red blood cells. We also quantified levels of monounsaturated fatty acids from the ω9 series (C16:1, C18:1, C20:1, C22:1, C24:1) and polyunsaturated long-chain fatty acids from the ω3 (C18:3, C18:4, C20:5, C22:5, C22:6), ω6 (C18:2, C18:3, C20:2, C20:3, C20:4, C22:2, C22:4, C22:5) and ω7 (C16:1, C18:1, C20:1) series in brain and plasma. We could not evidence any significant difference between abcd2−/− and their wild-type littermates (data not shown).

The high expression levels of ALDRP in DRG and the defective spinal reflex of abcd2−/− highlight this particular cell population as a target to identify a biochemical phenotype (90% of the cells in DRGs are neuronal bodies). We dissected DRGs from 5- to 6-day-old pups of *abcd2*−/− and wild-type littermates and quantified VLCFAs. We could indeed detect an accumulation of C26:0 in DRGs from abcd2−/− mice (Fig. 3I and J, $P < 0.002$). For comparison, we also analyzed DRGs from abcd1−/− and abcd1/abcd2−/− double mutants. Double mutants showed similar VLCFA levels than abcd2−/− mice. DRGs of abcd1−/− animals also showed slightly increased levels of C26:0, however, without reaching statistical significance. Thus, in DRGs, abcd2 seems to play the same role regarding C26:0 import/catabolism that abcd1 plays in most tissues.

Peripheral and central pathologies are associated with the neurological phenotype

Analysis of DRG cell number and size from semithin sections did not yield a significant difference between the abcd2−/− mice and their wild-type littermates either at 12 or 20 months of age (data not shown). However, electron microscopy examination revealed a specific pattern of degeneration, more evident at 20 months of age. Both in satellite cells and ganglia neurons, the accumulation of residual and zebra-like bodies was prominent (Fig. 4A). A significant number of mitochondria showed degenerative images and contained lipidic inclusions (Fig. 4C–E). We observed disturbed endoplasmic reticulum and Golgi apparatus, with dilatation and

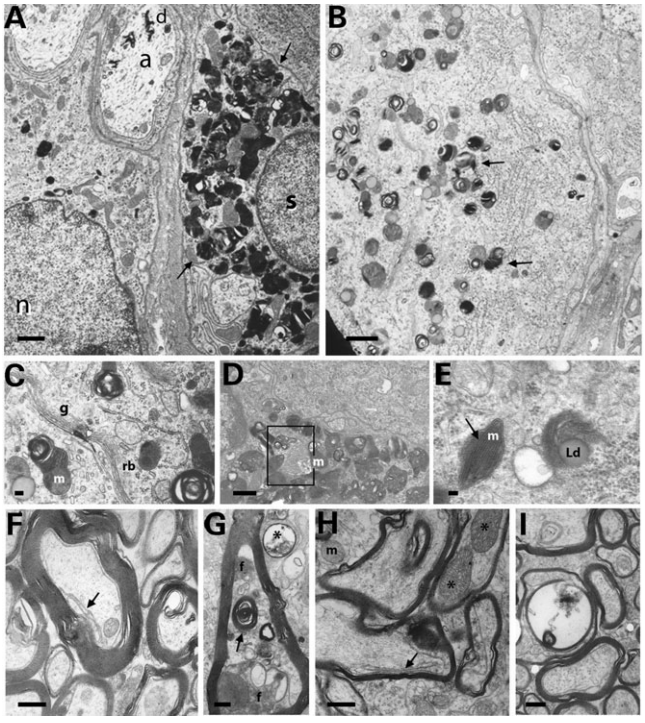

Figure 4. Pathological features on DRG cells in aldr−/− mice at 20 months of age. (**A**) High number of zebra bodies filling up a satellite cell (s). a: axon containing electron dense debris; n: ganglion cell nucleus. (**B**) Polymorphous residual and zebra-like bodies in cytoplasm of a ganglion cell (arrows). (**C**) Abnormal mitochondria with a lipid droplet and circular cristae in a ganglion cell (m). Fragmentation of Golgi cisternae (g). rb: residual body. (**D**) Mitochondria containing lipidic residual bodies in satellite cells. (**E**) In a ganglionar cell, mitochondria (m) with paracristallin profile (arrow) resulting from the juxtaposition of parallel-stacked cristae. In the vicinity, a lipid droplet (Ld) with an accumulation of filamentous, proteinaceous material. (**F**) Decompactation of axolemma (arrow). (**G**) Axonal degeneration: involution of the cellular organites with the formation of a fibrillar body (f) and myelin-like bodies (arrow); numerous vacuoles. Empty fiber (asterisk). (**H**) Myelin remnants in the Schwann cell, resulting in a fibrillar and granular body (f). Axolemma decompactation (arrow). Note two giant mitochondria (asterisks). (**I**) An empty myelinated fiber containing two myelin bodies. Scale bars: 1 μm (A and B); 0.1 μm (C–E); 0.5 μm (F–I).

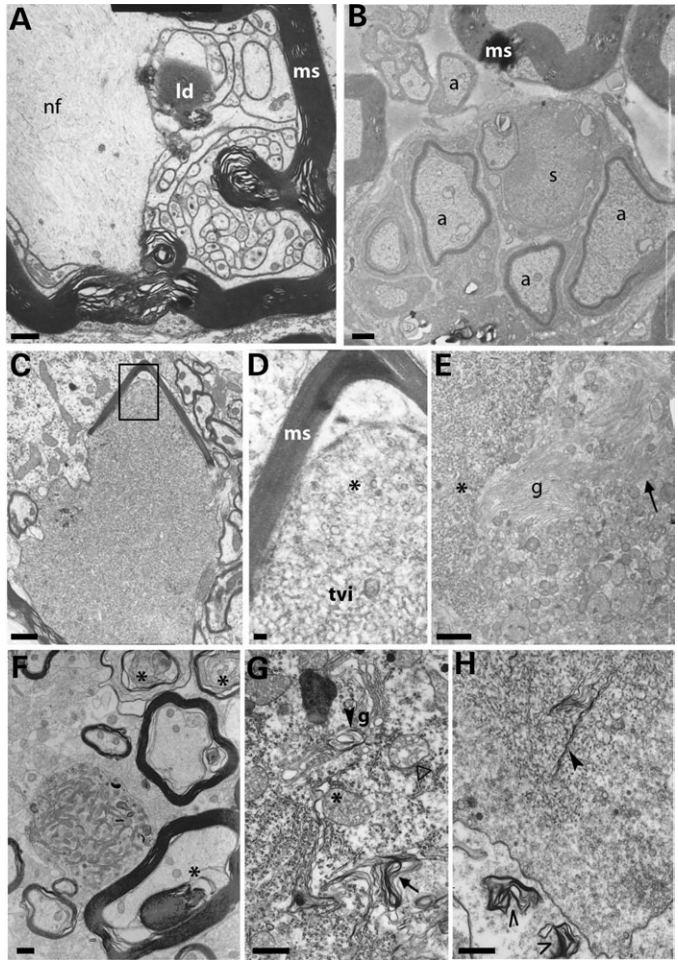

Figure 5. Pathological features in spinal cord, ventral horn gray matter of aldr−/− mice at 20 months of age, except (**B**). (**A**) Axonal sprouting within a large axon filled with neurofilaments (nf) surrounded by myelin sheath (ms), lipid droplet (ld). (B) Axonal sprouting consistent with axonal regeneration in sciatic nerve. a: axon; s: Schwann cell nuclei. (**C**) Dense, degenerating axoplasm focally surrounded by distorted myelin. (**D**) Higher magnification of the region within the square in (C), showing tubulo-vesicular inclusions (tvi) and fragmented smooth ER (asterisk). ms: myelin sheath. (**E**) Motor neuron cell body with hypertrophy of abnormal Golgi (g) cisternae associated to fragmented smooth ER (asterisk). Mitochondrial enlargement and densification of cristae (arrows). (**F**) At the image center, enlargement of a non-myelinated fiber, with accumulation of organelles. Note myelinated degenerating axons, with decompactation of axolemma (asterisk). (**G**) In neurons, lamellar bodies derived from altered Golgi (g) and rough endoplasmic reticulum (arrows). Note mitochondria with tubular cristae (asterisk) and ring-shaped alteration (white arrow). (**H**) Remnants of the Golgi apparatus in the form of lamellae (arrows), in a zone with small smooth ER vacuoles. Two lamellated bodies within an axonal fiber (open arrows). Scale bars: 1 μm (A–C, E and F); 0.1 μm (D); 0.5 μm (G and H).

fragmentation of channels and cisterns (Fig. 4C). The number of lysosomes was increased significantly, suggesting a high activation of the degradation processes. We encountered frequently axonal degenerative features, including axolemma decompactation (Fig. 4F–I).

In spinal cord dorsal and ventral columns, histological abnormalities not demonstrable at 12 months of age became evident in abcd2−/− mice at 20 months of age. Analysis of semithin sections showed fields of axonal spheroid degeneration comparable to those observed in abcd1−/− knock-out mice (21) (data not shown). Axonal degeneration and regeneration processes were often encountered in the form of axonal sprouting (Fig. 5A), consistent with findings of onion bulbs in sciatic nerve (Fig. 5B). Golgi apparatus fragmentation in the form of tubulo-vesicular inclusions was found in axons and neuronal cell bodies (Fig. 5C–E). Mitochondria abnormalities were frequent (Fig. 5E and G), as well as focal accumulation of organelles, a sign of disturbed axoplasmic flow (Fig. 5F). We then studiedthe dorsal columns of the spinal cord by immunohistochemical techniques. By Sudan black staining, we commonly evidenced axonal swellings (Fig. 6G and H), lesions that were often filled with ubiquitinated APP and synaptophysin accumulations, as revealed by analysis of serial sections (Fig. 6E–F and I–L). As a consequence, reactive astrogliosis appeared (Fig. 6A–D). The first signs of pathology were detected at 12 months in spinal cords and consisted on APP and synapthophysin accumulations in

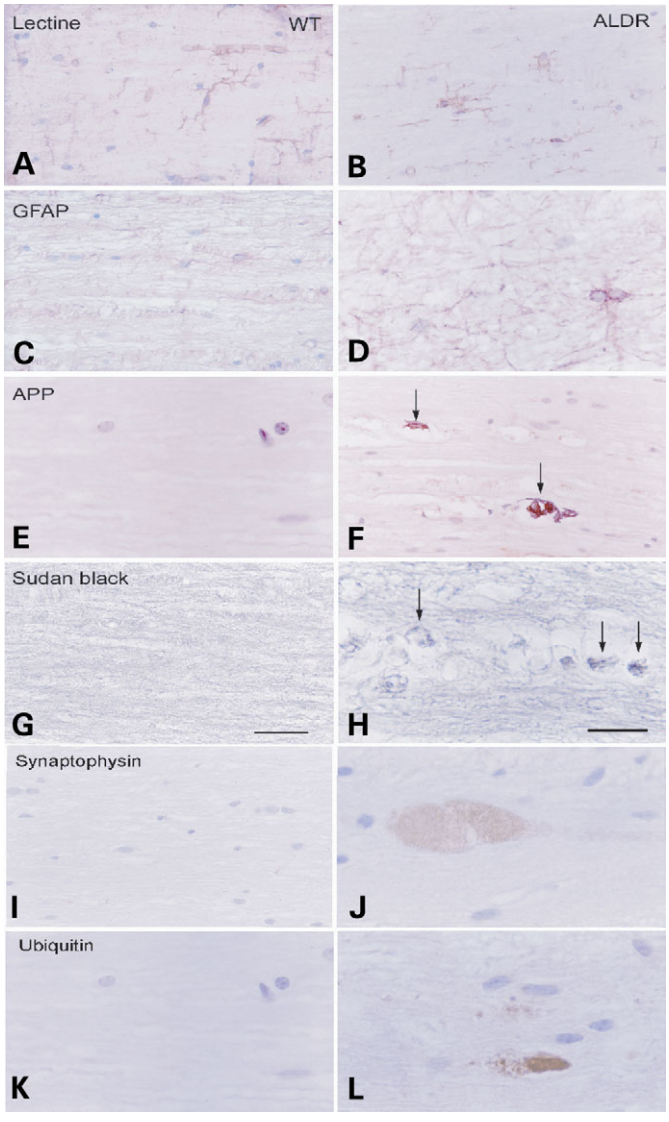

Figure 6. Gliosis, myelin and axonal pathology in spinal cord in aldr−/−. Longitudinal sections of the dorsal spinal cord in wild-type and aldr−/− and control littermates at the age of 20 months, processed for glial GFAP, lectin *L. esculentum*, APP, Sudan black and synaptophysin. (**A**–**D**) Reactive astrogliosis is observed in aldr−/− mice when compared with littermate controls. In (**E** and **F**), APP deposits are seen in axonal swellings in aldr−/− mice. This is accompanied by lipidic debris of myelin, as revealed with Sudan black in (**G** and **H**). In (**I** and **J**), abnormal fibers filled with synaptophysin are found in aldr−/− mice. Synaptophysin and APP deposits are ubiquitinated (**K** and **L**).

axonal swellings. The same type of immunostanings used for the spinal cord were used for the brain, without revealing any significant difference to wild-type littermates. Neither Nissl-staining could detect major neuroanatomical alterations. All brain nuclei were present and not markedly different from the wild-type littermates, indicating normal brain development in the abcd2−/− mice (data not shown).

Ataxia is commonly attributed to altered output from the cerebella cortex or from deep cerebella nuclei (22). Given the ataxic phenotype of the abcd2 −/− mice, we examined the cerebellum, using histological stainings (Nissl). At 12 months of age, the abcd2−/− cerebellum showed no major changes in appearance of the molecular, Purkinje cell and granule cell layers, as well as normal foliation and cytoarchitecture (data not shown). However, at 20 months of age, we detected gaps in the Purkinje cell monolayer in Nissl-stained sections (Fig. 7A and B). Immunohistochemistry against calbindin (D28-K) confirmed atrophy or death of Purkinje cells (Fig. 7C and D). A clear reduction of non-phosphorylated neurofilaments in Purkinje cells (SMI 32 antibody) (23) indicated reduced dendritic arborization (Fig. 7E and F). Fibrillary acidic protein (GFAP)-staining revealed an increased frequency of local spots of GFAP upregulation in the molecular layer of the cerebellum (Fig. 7E and F). These GFAP 'hot-spots' are likely to indicate a local degeneration of Purkinje cells with concomitant local reactive gliosis.

It is noteworthy that all the pathological changes noticed by ultrastructural or immunohistochemical techniques in abcd2−/− mice at DRGs, spinal cords and cerebellar sites were presented in the same extent, intensity and age by abcd1 deficient mice. Double mutants showed a more severe involvement and earlier onset of pathological signs, evidenced from 12 months onwards.

DISCUSSION

We present a model of late-onset, slowly progressive neuronal degeneration presumably caused by chronic accumulation of VLCFAs and/or other lipid metabolites due to ALDRP/ABCD2 inactivation.

On the basis of close sequence homology between *abcd2/aldr* and its paralog *abcd1/ald*, functional redundancy has been repeatedly suggested from the moment of its identification (24). Indeed, *abcd2* is able to correct the VLCFAs accumulation due to *abcd1* loss of function when overexpressed *in vitro* (15,16) and *in vivo* (18). In addition, overexpression of *abcd3* corrects VLCFAs levels *in vitro*, although its inactivation in the mouse does not lead to VLCFAs accumulation (17). Similarly, we could not detect higher levels of VLCFAs in neural tissue of abcd2−/− mice (18), thus leaving open the question of the true role of *abcd2* in relation to VLCFAs catabolism.

In the current work, we extended the biochemical analysis further to demonstrate a significant accumulation of VLCFAs in DRGs of abcd2−/− mice, together with normal levels of other peroxisomal metabolites. Thus, we present compelling evidence of a redundant biochemical function between the two transporters in the mouse. The normal levels of VLCFAs in brain and spinal cords of abcd2 mutants may be due to the fact that low numbers of cells express ALDRP (only one-fourth of the cells in total CNS homogenates are neurons, whereas 90% of the cells in DRGs are neurons), or alternatively, that its biochemical role regarding VLCFAs transport is quantitatively less important at the precise time point of analysis (8 months in whole neural tissue homogenates versus 5-day-old DRGs). It is worth noting that this biochemical abnormality in DRG neurons in abcd2−/− newborns correlates with a differential electromyographical phenotype against abcd1-deficient mice in adulthood. Indeed, ALD mice neither significantly

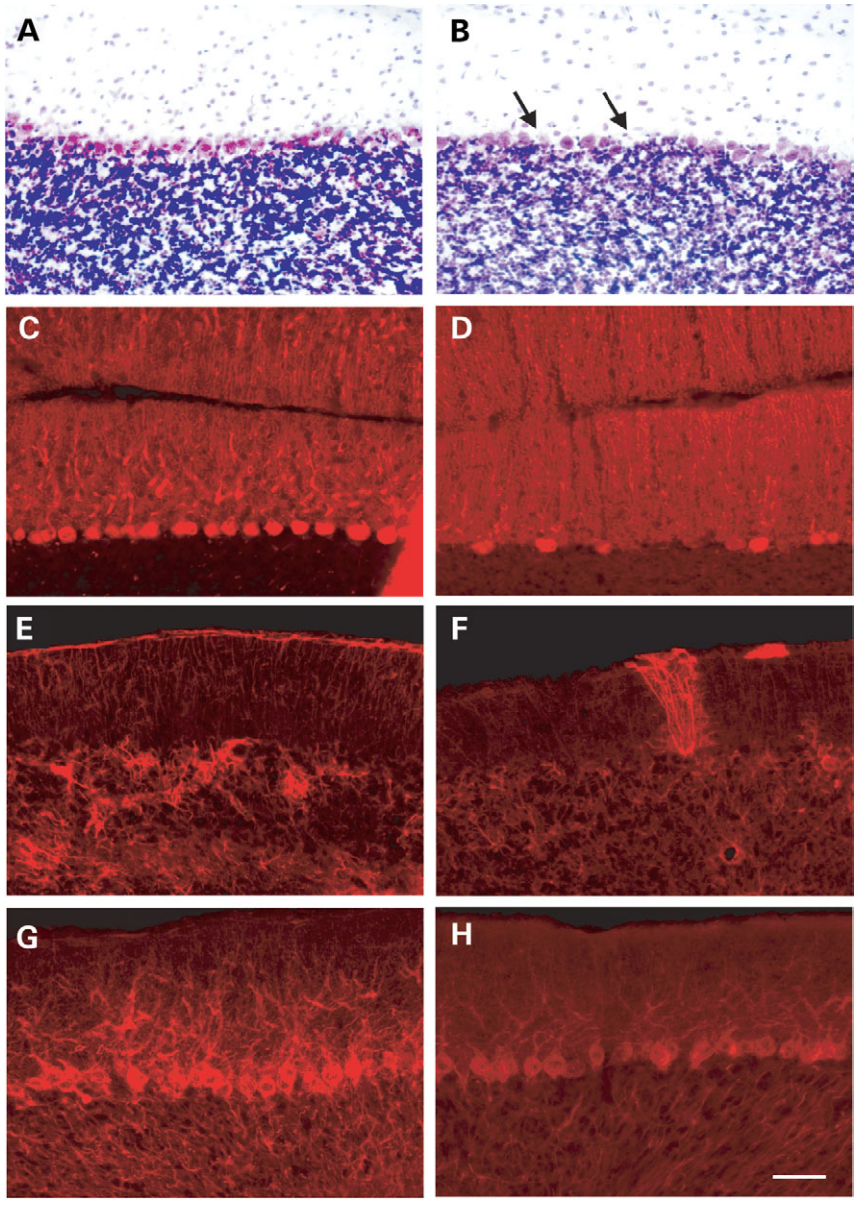

Figure 7. Cerebellar pathology in aldr−/− mice at 20 months of age. (**B**) Loss of Purkinje cell somata evidenced by Nissl staining (arrowheads). (**D**) Focal loss of staining with anti-calbindin D28K in the aldr−/− mice. (**F**) Focal upregulations of GFAP expression in aldr−/−. (**H**) Strong reduction of non-phosphorylated neurofilaments in Purkinje cells was seen by staining with anti-SMI32. (**A**, **C**, **E** and **G**) Images from wild-type littermate controls. Scale bar: 50 μm.

accumulated VLCFAs nor presented altered H-waves. The contrasting electromyographical phenotypes of abcd1- and abcd2−/− mice illustrate the complementary functions shared by the two transporters.

We face a different scenario when analyzing mouse fibroblasts. Most likely, because expression levels of abcd2 mRNA are rather low, inactivation of abcd2 neither leads to impairment of β-oxidation capacity nor to accumulation of VLCFAs. However, in a double mutant abcd1−/abcd2−/− context, accumulation of VLCFAs is significantly higher than in single abcd1- mutants, without additional impairment in peroxisomal degradation capacity. This might indicate that in this particular cell type and in the absence of ABCD1, ABCD2 is involved in a metabolic pathway other than degradation of VLCFAs, which leads to a secondary accumulation of VLCFAs. This is in agreement with results provided in McGuinness *et al.* (25), where the authors find normal VLCFAs β-oxidation levels in ALD mouse tissues and thus claim that the relationship between ALDP function and VLCFA metabolism is merely indirect.

Our findings demonstrate that loss of abcd1, the gene responsible for a demyelinating disease, leads to axonal degeneration, with degenerative features compatible with axonal transport impairment and to Purkinje cell loss in mice. This comes as no surprise if we consider that even in primary myelin disorders, such as multiple sclerosis (26), or

in the absence of a major myelin protein CNPase axonal loss occur (27). Those axonal swellings and degeneration have consequently been attributed to loss of oligodendroglia/myelin support. Thus, oligodendrocytes communicate in some way with the underlying axon and support axonal function. In contrast, inactivation of its predominantly neuronal expressed paralog abcd2 leads not only to the same type of phenotype, neuronal and axonal degeneration but also to astrocyte activation and gliosis. Along with these lines, at the histopathological level and by the means we have used, it has not been possible to clearly discriminate between the phenotypes of both mutants. Abcd1 and abcd2 deficient mice present very similar (in quality and quantity/number and morphology) accumulations of APP and synaptophysin in axonal swellings, astrogliosis in spinal cord and cerebellum and loss of Purkinje cells in cerebellum, despite the lack of detectable abnormalities in the cerebral cortex.

It is through neurological and electrophysiological testing that we can discriminate between the roles of both transporters. Abcd2−/− mice present defective spinal reflexes and ataxic phenotype, similar to the mouse models of Friedreich ataxia or vitamin E deficiency (28,29), at an age when Abcd1-mice still do well. The differences in expression pattern most likely account for a differential vulnerability/different target cellular populations, thus resulting in a different phenotypic outcome. Although *abcd1* and *abcd2* genes demonstrate functional redundancy that extends beyond their shared biochemical roles, abcd2−/− mice display abnormalities not observed in abcd1-mutant mice, revealing that *abcd1* and *abcd2*, or their genetic regulation, are not equivalent. For instance, the hyperactivity/lack of habituation phenotype displayed by aldr−/− mice deserves further study, as disturbance of higher cognitive functions could be underlying this pathological feature. Taking all pathological findings together, we conclude that abcd2−/− mice develop a late-onset spinocerebellar ataxia, with impaired propioception most likely due to neuronal degenerative processes at the DRG level or to synaptic defects in spinal cord. To date, no human syndrome compatible with this phenotype has been linked to the *ABCD2* locus at 12q1.1–1.2. Thus, description of the phenotype in mice might contribute to identifying patients suffering from a similar condition, i.e. an autosomal recessive peripheral neuropathy with cerebellar involvement, but without elevation of VLCFA in plasma or fibroblasts.

An interesting feature found in both ALD and ALDR mouse models is the presence of ultrastructural alterations of mitochondria in axons and neuronal bodies. The degradation of fatty acids in mammals takes place in mitochondria and peroxisomes. Very-long-chain and certain branched-chain fatty acids are first chain-shortened in peroxisomes, and subsequently, oxidized to completion in mitochondria via the β-oxidation pathway. A growing body of evidence suggests that mitochondria is playing a significant role in the pathogenesis of peroxisomal disease and that a relevant cross-talk connects both organelles. For instance, β-oxidation activity for VLCFAs is still present to ∼60% in patients and mouse ALD-deficient fibroblasts (30–32); it is surprisingly normal in mouse tissues lacking ALDP (25) and even still present up to 20% in some cases in Zellweger patients fibroblasts (Wanders, personal communication). These findings are consistent with an overlapping or compensatory role between both organelles. Indeed, mitochondrial anomalies are observed in liver of mice with a total ablation of peroxisomal β-oxidation (inactivation of multifunctional proteins 1 and 2) (33). Moreover, functional and ultrastructural mitochondrial abnormalities have been found in the liver of a Zellweger syndrome mouse model (34,35), as well as in human Zellweger syndrome, including lipidic inclusions (36). Recently, the mitochondrion has also been implicated in the pathogenesis of X-ALD in mice and human. Lipidic intramitochondrial inclusions have been observed in atrophic neurons of DRG in patients with AMN, the adult form of X-ALD (37). Functional and structural alterations of mitochondria in adrenal cortex as a result of loss of ALDP are found in the X-ALD mouse model (25). These lipidic inclusions and condensation of cristae resemble the anomalies we have found in the neural tissue of both ALDP and ALDRP deficient mice. These signs of mitochondrial stress may reflect an attempt of the organelle to 'back-up' for the impaired peroxisomal function or simply an overload of the mitochondria with substrates that should have been degraded in peroxisomes. Defective mitochondria may lead to a failure of ATP-dependent axoplasmic transport with consequent 'dying-back' axonal degeneration. Indeed, structurally abnormal mitochondria in affected axons are associated with segmental axonal swelling and impairment of anterograde and retrograde transport in a mouse model of HSP (38). Mitochondrial damage has also been found associated with aberrant sprouting and synapse loss in AD and dementia with Lewy bodies (39). In our models, the presence of axonal swellings that accumulate neurofilaments and organelles suggests a similar pathogenetic mechanism. In addition, prominent in the ALD and ALDR mouse models is the tubulo-vesicular inclusions derived from endoplasmic reticulum and Golgi fragmentation. Interestingly, fragmentation of Golgi apparatus is found in sporadic amyotrophic lateral sclerosis (40,41) and in mouse models of tauopathies, where it has been associated with neuronal atrophy and non-apoptotic cell death (42). Thus, the neurodegenerative features we have identified in ALD and ALDR mouse models placed them in a common path with other major neurodegenerative diseases.

The link between defective VLCFAs catabolism and pathogenesis is not obvious in X-ALD. The incorporation of excess of VLCFAs into cell membranes might impair membrane stability (43) or perturb their microenvironment, resulting in dysfunction and death of vulnerable cells (44,45). Others showed that cells exposed to C26:0 produce higher levels of reactive oxygen species (46). While this article was in preparation, a direct correlation between accumulation of saturated VLCFAs in brain white matter and disease severity in human X-ALD patients has been reported, shedding some light into the issue (47). Thus, accumulation of VLCFAs in DRGs of abcd2−/− mice may increase the vulnerability to this particular cellular population to neurodegeneration. VLCFAs are found as lateral chains of complex lipids, such as phosphatidylcholine or phosphatidylethanolamine, thus playing a main structural role as components of cellular membranes. In neural membranes, a strict balance between free and esterified fatty acids is necessary, not only for normal membrane composition, integrity and function but also for the optimal

activity of the membrane-bound enzymes, receptors and ion channels involved in normal signal-transduction processes. We propose that the composition, maintenance or recycling process of myelin and neuronal/axonal membrane might be disturbed in the ALD and ALDR models, leading to impaired axono-glia communication, which would be detrimental for both interconnected compartments. Crucial to understanding of ALD and ALDR pathogenesis is to elucidate the mechanisms by which impaired peroxisomal function(s) or VLCFAs accumulation results in axonal degeneration, with features compatible with axonal transport impairment. VLCFAs levels have been found to be increased in X-ALD brain gangliosides (48), which might contribute to pathogenesis. Another plausible link may focus on the proteolipid protein (PLP/DM20), the main component of CNS myelin, accounting for $>50\%$ of the total protein of this membrane. PLP is a palmitoylated protein that contains mainly palmitic, oleic and stearic acids covalently bound as acyl chains. In adrenoleukodystrophy patients, the proportions of saturated VLCFAs bound to PLP have been found to be increased at the expense of oleic acid (49). Because covalently bound fatty acids contribute to the tertiary structure of PLP in aqueous medium (50), this altered fatty acid composition may influence its physical or biological properties, compromising stability of PLP itself or its insertion in the myelin sheath. Indeed, recent evidence indicates a severe impairment of fast axonal transport system in the PLP/DM20 deficient mouse (51), thus underscoring the importance of a healthy membrane for axonal function.

MATERIALS AND METHODS

Mouse generation, breeding and genotyping

The abcd2−/− mice were generated by inactivation of the *abcd2* gene by classic homologous recombination. The *abcd2* genomic sequence was isolated from a 129 mouse genomic library. Two fragments of the *abcd2* gene were cloned into a pPNT backbone vector that contained a neomycin selection cassette flanked by *Lox*P sites (Fig. 1A). The linearized targeting vector was transfected into male R1 embryonic stem cells derived from 129 mouse strain. Double selection was performed with G418 and ganciclovir, and drug-resistant clones were screened for homologous recombination by Southern blotting (Fig. 1B). We obtained three recombinant clones, out of 302, resistant to neomycin, which were injected into blastocysts from C57BL/6 mice. Chimeric male pups were bred with C57BL/6 females to confirm germ-line transmission. DNA extracted from tails was used for PCR-based genotyping, using standard protocols. Primers used for genotyping were as follows: a common primer (5′-GAG CTAGTGTCATTGTTCTG-3′) used together with a WT-specific (5′-TAACCTGCTAGTTCAGTGAT-3′) or a KO-specific (5′-TGCAATCCATCTTGTTCAATG-3′). The *abcd1* gene inactivation has been described (30). To obtain double heterozygous mutants, we crossed abcd1$^{-/+}$ females with abcd2$^{-/-}$ mice. Double heterozygotes were intercrossed to obtain double knock-out mice and wild-type littermate controls; the offspring obeyed Mendelian ratios. Results described in this manuscript are derived from mice on a mixed C57BL/6J/129Sv background ($\sim$87% C57BL/6J and 13%129Sv). Crucial experiments (locomotor tests and EMG) have been confirmed with pure C57BL/6J background mice. Histology, morphometric, behavioral testing and electrophysiological experiments were performed in a blind way with respect to the animal's genotype. All methods employed in this work are in accordance with the Guide for the Care and Use of Laboratory Animals published by the US National Institutes of Health (NIH Publications no. 85-23, revised 1996).

Behavior tests

All experiments were performed with naïve male animals, which were kept on a 12 h light/dark cycle.

Open field and rotarod tests

Coordination, balance and motor skill acquisition were tested using an accelerated rotaring rod (Panlab, Barcelona, Spain) test, as described previously (21). In brief, mice were placed on the rod in a routine of four trials per day for a period of 4 days. The rod accelerated from 4 to 40 r.p.m. in 5 min and remained at maximum speed two more minutes. Animals were scored for their latency to fall (in seconds) for each trial and rested a minimum of 10 min between trials to avoid exhaustion. Results were analyzed by a repeated-measure ANOVA test, considering three factors: days (fixed), genotype (fixed) and animals (variable), nested in genotype and crossed with days. Spontaneous ambulation in an open field was recorded during a 15 min period as described (21).

Horizontal bar cross test

The bar cross test is carried out using a wooden bar of 100 cm in length and 2 cm in width (diameter). This bar is just wide enough for mice to stand on with their hind feet hanging over the edge such that any slight lateral misstep will result in a slip. The bar is elevated 50 cm from the bench surface, so that animals do not jump off, yet are not injured upon falling from the bar. To eliminate the novelty of the tasks as a source of slips, all animals were given four trials on the bar at the beginning of the testing session. By the fourth trial, control animals ran the bar with not more than two slips. In the experimental session, the number of hind limb lateral slips and falls from the bar and the time to reach the platform were counted on four consecutive trials. If an animal fell, it was placed back on the bar at the point at which it fell and was allowed to complete the task. The bar was cleaned with ethanol after each animal had crossed it.

Fibroblast culture and biochemical measurements

Primary fibroblast cultures were derived from mutant mice and their control littermates and grown at 37°C in 5% CO_2 in DMEM, supplemented with fetal calf serum (10%), penicillin (100 U/ml) and streptomycin (100 U/ml). Cultures were grown to confluence on monolayer. Fatty acid β-oxidation was determined by measuring the capacity of the intact cells to degrade ^{14}1-C-labeled fatty acids (C26:0) to water-soluble products, essentially as described (52). Specific activity was expressed as picomoles of $^{14}CO_2$ released per hour per

milligram of protein. Total cellular VLCFAs fatty acids were analyzed using electrospray ionization-tandem mass spectrometry (ESI-MS), as described recently (53). Branched-chain fatty acids in plasma and liver were analyzed using GC-MS (54). Total monounsaturated and polyunsaturated fatty acids in brain and plasmalogens in erythrocytes were measured by GC analysis (55).

Statistical analysis

Data are expressed as mean ± SD. Statistical significance was evaluated using ANOVA tests (Statview Package 5). The results were considered significant at $P < 0.01$.

Electrophysiological recordings

Electromyograms were performed at Neurofit (Strasbourg, France) using a Neuromatic 2000M apparatus (Dantec, Les Ulis, France). Mice were anesthetized with intraperitoneal injection of 60 mg/kg ketamine chlorohydrate (Imalgene 500°; Rhone-Biomerieux, Lyon, France). Distal latency and amplitude of M- and H-waves were recorded in the plantar hind paw muscle after sciatic nerve stimulation.

Electron microscopy

Mice were anesthetized as described earlier and perfused with a 4% PFA and 3% glutaraldehyde (Fluka) in phosphate buffered (pH 7.4, 0.1 M) solution. Spinal cord, DRG and cerebrum were dissected and fixed overnight. Tissue was post-fixed for 1 h in 1% osmium tetroxide in phosphate buffer, dehydrated in serial ethanol solutions and embedded in an araldite–epon mixture. Embedded tissues were then placed at ±60°C for 2 days to polymerize. Transverse semi-thin sections, 1 μm in thickness, were prepared with an ultramicrotome and stained with Toluidine blue. Ultrathin sections (50 nm) were investigated on a Philips C12-208 electron microscope at 80 kV.

In situ hybridization

ISH on mouse embryos (whole mounts) and radioactive ISH on post-natal frozen CNS were performed as described (56). The antisense RNA probes used contained the whole cDNA sequence of the *abcd1* gene and the C-terminal half of the *abcd2* gene, as previously described (19).

Immunohistochemistry

Mice were perfused with a 4% PFA solution. Spinal cords were embedded in paraffin and serial sections, 5 μm thick, were cut in the longitudinal plane with a sliding microtome. The sections were stained with hematoxylin and eosin, Luxol fast blue-Klüver-Barrera and Sudan black or processed for immunohistochemistry to glial GFAP (Dako, rabbit polyclonal, 1:500), ubiquitin (Dako, rabbit polyclonal, 1:500), APP (Boehringer, 1:10) and synaptophysin (Dako, monoclonal, 1:500). Lectin *Lycopericon esculentum* (Sigma, L-0651, 1:200) was used as a marker for microglial cells. The sections were incubated with the modified labeled streptavidin (LSAB) technique (DAKO LSAB2 System Peroxidase). The number of abnormal specific profiles was quantified in every tenth section for each particular stain. Five sections corresponding to the dorsal columns of the spinal cord were analyzed per animal and per stain. For analysis of the cerebellar pathology, frozen sections were used, which were incubated as free floating sections with antibodies against calbindin D28K (Swant, 1:1000), SMI32 (Sternberger monoclonals, 1:1000) and GFAP (Dako, 1:1000). The staining was visualized with AlexaFluor 568 secondary antibodies (Molecular Probes).

ACKNOWLEDGEMENTS

We are indebted to Drs Deborah Bartholdi, Stéphane Fourcade, Sander Houten, Fredoen Valianpour, Marisa Girós, Montse Ruiz and Teresa Pàmpols for fruitful discussions. ALD mutant mice were a kind gift of Dr Kirby Smith (KKI, Baltimore, MD). We thank Sandra Metz for graphical work; C. Kretz, L. Reutenauer, J. Ruiter, H. Overmars, H. Rush, E. Vega, R. Blanco and M. Carmona for priceless technical assistance and Drs Marianne Lemeur, Elisabeth Metzger, Andrée Dierich and the staff at the IGBMC animal facility for mouse care. This study was supported by funds from the Institut National de la Santé et de la Recherche Médicale, the Centre National de la Recherche Scientifique, the European Commission contract no. LSHM-CT2004-502987, the Association Française contre les Myopathies (Grant no. 9315), the European Leukodystrophy Association and the Spanish Fondo de Investigacion Sanitaria (FIS, Ministerio de Sanidad project no. 01/1667).

Conflict of Interest statement. None declared.

REFERENCES

1. De Duve, C. and Baudhuin, P. (1966) Peroxisomes (microbodies and related particles). *Physiol. Rev.*, **46**, 323–357.
2. Wanders, R.J. and Tager, J.M. (1998) Lipid metabolism in peroxisomes in relation to human disease. *Mol. Aspects Med.*, **19**, 69–154.
3. Subramani, S. (1998) Components involved in peroxisome import, biogenesis, proliferation, turnover, and movement. *Physiol. Rev.*, **78**, 171–188.
4. Gould, S.J. and Valle, D. (2000) Peroxisome biogenesis disorders: genetics and cell biology. *Trends Genet.*, **16**, 340–345.
5. Citkowitz, E. and Holtzman, E. (1973) Peroxisomes in dorsal root ganglia. *J. Histochem. Cytochem.*, **21**, 34–41.
6. McKenna, O., Arnold, G. and Holtzman, E. (1976) Microperoxisome distribution in the central nervous system of the rat. *Brain Res.*, **117**, 181–194.
7. Arnold, G. and Holtzman, E. (1978) Microperoxisomes in the central nervous system of the postnatal rat. *Brain Res.*, **155**, 1–17.
8. Bradke, F. and Dotti, C.G. (1997) Neuronal polarity: vectorial cytoplasmic flow precedes axon formation. *Neuron*, **19**, 1175–1186.
9. Ishikawa, T., Kawai, C., Sano, M. and Minatogawa, Y. (2001) Peroxisomes exist in growth cones and move anterogradely and retrogradely in neurites of PC12D cells. *Exp. Cell Res.*, **266**, 260–269.
10. Hyde, S.C., Emsley, P., Hartshorn, M.J., Mimmack, M.M., Gileadi, U., Pearce, S.R., Gallagher, M.P., Gill, D.R., Hubbard, R.E. and Higgins, C.F. (1990) Structural model of ATP-binding proteins associated with cystic fibrosis, multidrug resistance and bacterial transport. *Nature*, **346**, 362–365.
11. Dean, M. and Allikmets, R. (1995) Evolution of ATP-binding cassette transporter genes. *Curr. Opin. Genet. Dev.*, **5**, 779–785.

12. Mosser, J., Douar, A.M., Sarde, C.O., Kioschis, P., Feil, R., Moser, H., Poustka, A.M., Mandel, J.L. and Aubourg, P. (1993) Putative X-linked adrenoleukodystrophy gene shares unexpected homology with ABC transporters. *Nature*, **361**, 726–730.
13. Shani, N., Watkins, P.A. and Valle, D. (1995) PXA1, a possible *Saccharomyces cerevisiae* ortholog of the human adrenoleukodystrophy gene. *Proc. Natl Acad. Sci. USA*, **92**, 6012–6016.
14. Hettema, E.H., Girzalsky, W., van Den Berg, M., Erdmann, R. and Distel, B. (2000) *Saccharomyces cerevisiae* pex3p and pex19p are required for proper localization and stability of peroxisomal membrane proteins. *EMBO J.*, **19**, 223–233.
15. Braiterman, L.T., Zheng, S., Watkins, P.A., Geraghty, M.T., Johnson, G., McGuinness, M.C., Moser, A.B. and Smith, K.D. (1998) Suppression of peroxisomal membrane protein defects by peroxisomal ATP binding cassette (ABC) proteins. *Hum. Mol. Genet.*, **7**, 239–247.
16. Netik, A., Forss-Petter, S., Holzinger, A., Molzer, B., Unterrainer, G. and Berger, J. (1999) Adrenoleukodystrophy-related protein can compensate functionally for adrenoleukodystrophy protein deficiency (X-ALD): implications for therapy. *Hum. Mol. Genet.*, **8**, 907–913.
17. Silva-Zolezzi, I., Hebron, K., Mihalik, S., Thomas, G., Valle, D. and Jimenez-Sanchez, G. (2003) Abcd3−/− mice have a non-shivering thermogenesis defect related to a disturbance in fasting fuel homeostasis. *53rd Annual Meeting of the American Society of Human Genetics.* The American Society of Human Genetics, Los Angeles, California, Vol. Supplement to Vol. 73, p. 199.
18. Pujol, A., Ferrer, I., Camps, C., Metzger, E., Hindelang, C., Callizot, N., Ruiz, M., Pampols, T., Giros, M. and Mandel, J.L. (2004) Functional overlap between ABCD1 (ALD) and ABCD2 (ALDR) transporters: a therapeutic target for X-adrenoleukodystrophy. *Hum. Mol. Genet.*, **13**, 2997–3006.
19. Troffer-Charlier, N., Doerflinger, N., Metzger, E., Fouquet, F., Mandel, J.L. and Aubourg, P. (1998) Mirror expression of adrenoleukodystrophy and adrenoleukodystrophy related genes in mouse tissues and human cell lines. *Eur. J. Cell Biol.*, **75**, 254–264.
20. Gilman, S. (1969) The mechanism of cerebellar hypotonia. An experimental study in the monkey. *Brain*, **92**, 621–638.
21. Pujol, A., Hindelang, C., Callizot, N., Bartsch, U., Schachner, M. and Mandel, J.L. (2002) Late onset neurological phenotype of the X-ALD gene inactivation in mice: a mouse model for adrenomyeloneuropathy. *Hum. Mol. Genet.*, **11**, 499–505.
22. Klockgether, T. and Evert, B. (1998) Genes involved in hereditary ataxias. *Trends Neurosci.*, **21**, 413–418.
23. Sternberger, L.A. and Sternberger, N.H. (1983) Monoclonal antibodies distinguish phosphorylated and nonphosphorylated forms of neurofilaments *in situ*. *Proc. Natl Acad. Sci. USA*, **80**, 6126–6130.
24. Lombard-Platet, G., Savary, S., Sarde, C.O., Mandel, J.L. and Chimini, G. (1996) A close relative of the adrenoleukodystrophy (ALD) gene codes for a peroxisomal protein with a specific expression pattern. *Proc. Natl Acad. Sci. USA*, **93**, 1265–1269.
25. McGuinness, M.C., Lu, J.F., Zhang, H.P., Dong, G.X., Heinzer, A.K., Watkins, P.A., Powers, J. and Smith, K.D. (2003) Role of ALDP (ABCD1) and mitochondria in X-linked adrenoleukodystrophy. *Mol. Cell. Biol.*, **23**, 744–753.
26. Bjartmar, C., Wujek, J.R. and Trapp, B.D. (2003) Axonal loss in the pathology of MS: consequences for understanding the progressive phase of the disease. *J. Neurol. Sci.*, **206**, 165–171.
27. Lappe-Siefke, C., Goebbels, S., Gravel, M., Nicksch, E., Lee, J., Braun, P.E., Griffiths, I.R. and Nave, K.A. (2003) Disruption of Cnp1 uncouples oligodendroglial functions in axonal support and myelination. *Nat. Genet.*, **33**, 366–374.
28. Simon, D., Seznec, H., Gansmuller, A., Carelle, N., Weber, P., Metzger, D., Rustin, P., Koenig, M. and Puccio, H. (2004) Friedreich ataxia mouse models with progressive cerebellar and sensory ataxia reveal autophagic neurodegeneration in dorsal root ganglia. *J. Neurosci.*, **24**, 1987–1995.
29. Yokota, T., Igarashi, K., Uchihara, T., Jishage, K., Tomita, H., Inaba, A., Li, Y., Arita, M., Suzuki, H., Mizusawa, H. *et al.* (2001) Delayed-onset ataxia in mice lacking alpha-tocopherol transfer protein: model for neuronal degeneration caused by chronic oxidative stress. *Proc. Natl Acad. Sci. USA*, **98**, 15185–15190.
30. Lu, J.F., Lawler, A.M., Watkins, P.A., Powers, J.M., Moser, A.B., Moser, H.W. and Smith, K.D. (1997) A mouse model for X-linked adrenoleukodystrophy. *Proc. Natl Acad. Sci. USA*, **94**, 9366–9371.
31. Forss-Petter, S., Werner, H., Berger, J., Lassmann, H., Molzer, B., Schwab, M.H., Bernheimer, H., Zimmermann, F. and Nave, K.A. (1997) Targeted inactivation of the X-linked adrenoleukodystrophy gene in mice. *J. Neurosci. Res.*, **50**, 829–843.
32. Kobayashi, T., Shinnoh, N., Kondo, A. and Yamada, T. (1997) Adrenoleukodystrophy protein-deficient mice represent abnormality of very long chain fatty acid metabolism. *Biochem. Biophys. Res. Commun.*, **232**, 631–636.
33. Fan, C.Y., Pan, J., Usuda, N., Yeldandi, A.V., Rao, M.S. and Reddy, J.K. (1998) Steatohepatitis, spontaneous peroxisome proliferation and liver tumors in mice lacking peroxisomal fatty acyl-CoA oxidase. Implications for peroxisome proliferator-activated receptor alpha natural ligand metabolism. *J. Biol. Chem.*, **273**, 15639–15645.
34. Baumgart, E., Vanhorebeek, I., Grabenbauer, M., Borgers, M., Declercq, P.E., Fahimi, H.D. and Baes, M. (2001) Mitochondrial alterations caused by defective peroxisomal biogenesis in a mouse model for Zellweger syndrome (PEX5 knockout mouse). *Am. J. Pathol.*, **159**, 1477–1494.
35. Dirkx, R., Vanhorebeek, I., Martens, K., Schad, A., Grabenbauer, M., Fahimi, D., Declercq, P., Van Veldhoven, P.P. and Baes, M. (2005) Absence of peroxisomes in mouse hepatocytes causes mitochondrial and ER abnormalities. *Hepatology*, **41**, 868–878.
36. Sarnat, H.B., Machin, G., Darwish, H.Z. and Rubin, S.Z. (1983) Mitochondrial myopathy of cerebro-hepato-renal (Zellweger) syndrome. *Can. J. Neurol. Sci.*, **10**, 170–177.
37. Powers, J.M., DeCiero, D.P., Cox, C., Richfield, E.K., Ito, M., Moser, A.B. and Moser, H.W. (2001) The dorsal root ganglia in adrenomyeloneuropathy: neuronal atrophy and abnormal mitochondria. *J. Neuropathol. Exp. Neurol.*, **60**, 493–501.
38. Ferreirinha, F., Quattrini, A., Pirozzi, M., Valsecchi, V., Dina, G., Broccoli, V., Auricchio, A., Piemonte, F., Tozzi, G., Gaeta, L. *et al.* (2004) Axonal degeneration in paraplegin-deficient mice is associated with abnormal mitochondria and impairment of axonal transport. *J. Clin. Invest.*, **113**, 231–242.
39. Hashimoto, M. and Masliah, E. (2003) Cycles of aberrant synaptic sprouting and neurodegeneration in Alzheimer's and dementia with Lewy bodies. *Neurochem. Res.*, **28**, 1743–1756.
40. Gonatas, N.K., Stieber, A., Mourelatos, Z., Chen, Y., Gonatas, J.O., Appel, S.H., Hays, A.P., Hickey, W.F. and Hauw, J.J. (1992) Fragmentation of the Golgi apparatus of motor neurons in amyotrophic lateral sclerosis. *Am. J. Pathol.*, **140**, 731–737.
41. Stieber, A., Gonatas, J.O., Moore, J.S., Bantly, A., Yim, H.S., Yim, M.B. and Gonatas, N.K. (2004) Disruption of the structure of the Golgi apparatus and the function of the secretory pathway by mutants G93A and G85R of Cu, Zn superoxide dismutase (SOD1) of familial amyotrophic lateral sclerosis. *J. Neurol. Sci.*, **219**, 45–53.
42. Yoshiyama, Y., Zhang, B., Bruce, J., Trojanowski, J.Q. and Lee, V.M. (2003) Reduction of detyrosinated microtubules and Golgi fragmentation are linked to tau-induced degeneration in astrocytes. *J. Neurosci.*, **23**, 10662–10671.
43. Ho, J.K., Moser, H., Kishimoto, Y. and Hamilton, J.A. (1995) Interactions of a very long chain fatty acid with model membranes and serum albumin. Implications for the pathogenesis of adrenoleukodystrophy. *J. Clin. Invest.*, **96**, 1455–1463.
44. Bernheimer, H., Budka, H. and Muller, P. (1983) Brain tissue immunoglobulins in adrenoleukodystrophy: a comparison with multiple sclerosis and systemic lupus erythematosus. *Acta Neuropathol.* (*Berl.*), **59**, 95–102.
45. Powers, J.M. and Moser, H.W. (1998) Peroxisomal disorders: genotype, phenotype, major neuropathologic lesions, and pathogenesis. *Brain Pathol.*, **8**, 101–120.
46. Di Biase, A., Di Benedetto, R., Fiorentini, C., Travaglione, S., Salvati, S., Attorri, L. and Pietraforte, D. (2004) Free radical release in C6 glial cells enriched in hexacosanoic acid: implication for X-linked adrenoleukodystrophy pathogenesis. *Neurochem. Int.*, **44**, 215–221.
47. Asheuer, M., Bieche, I., Laurendeau, I., Moser, A., Hainque, B., Vidaud, M. and Aubourg, P. (2005) Decreased expression of ABCD4 and BG1 genes early in the pathogenesis of X-linked adrenoleukodystrophy. *Hum. Mol. Genet.*, **14**, 1293–1303.

48. Igarashi, M., Schaumburg, H.H., Powers, J., Kishmoto, Y., Kolodny, E. and Suzuki, K. (1976) Fatty acid abnormality in adrenoleukodystrophy. *J. Neurochem.*, **26**, 851–860.
49. Bizzozero, O.A., Zuniga, G. and Lees, M.B. (1991) Fatty acid composition of human myelin proteolipid protein in peroxisomal disorders. *J. Neurochem.*, **56**, 872–878.
50. Bizzozero, O.A. and Lees, M.B. (1986) Fatty acid acylation of rat brain myelin proteolipid protein *in vitro*: identification of the lipid donor. *J. Neurochem.*, **46**, 630–636.
51. Edgar, J.M., McLaughlin, M., Yool, D., Zhang, S.C., Fowler, J.H., Montague, P., Barrie, J.A., McCulloch, M.C., Duncan, I.D., Garbern, J. *et al.* (2004) Oligodendroglial modulation of fast axonal transport in a mouse model of hereditary spastic paraplegia. *J. Cell Biol.*, **166**, 121–131.
52. Wanders, R.J., Denis, S., Ruiter, J.P., Schutgens, R.B., van Roermund, C.W. and Jacobs, B.S. (1995) Measurement of peroxisomal fatty acid beta-oxidation in cultured human skin fibroblasts. *J. Inherit. Metab. Dis.*, **18** (Suppl. 1), 113–124.
53. Valianpour, F., Selhorst, J.J., van Lint, L.E., van Gennip, A.H., Wanders, R.J. and Kemp, S. (2003) Analysis of very long-chain fatty acids using electrospray ionization mass spectrometry. *Mol. Genet. Metab.*, **79**, 189–196.
54. Vreken, P., van Lint, A.E., Bootsma, A.H., Overmars, H., Wanders, R.J. and van Gennip, A.H. (1998) Rapid stable isotope dilution analysis of very-long-chain fatty acids, pristanic acid and phytanic acid using gas chromatography-electron impact mass spectrometry. *J. Chromatogr. B Biomed. Sci. Appl.*, **713**, 281–287.
55. Dacremont, G. and Vincent, G. (1995) Assay of plasmalogens and polyunsaturated fatty acids (PUFA) in erythrocytes and fibroblasts. *J. Inherit. Metab. Dis.*, **18** (Suppl. 1), 84–89.
56. Di Cunto, F., Imarisio, S., Hirsch, E., Broccoli, V., Bulfone, A., Migheli, A., Atzori, C., Turco, E., Triolo, R., Dotto, G.P. *et al.* (2000) Defective neurogenesis in citron kinase knockout mice by altered cytokinesis and massive apoptosis. *Neuron*, **28**, 115–127.